Electronic Supplementary Information for:

Structural evolution of imine-linked covalent organic frameworks and the NH_3 sensing performance

Fang Niu,[a] Zhen-Wu Shao,[a] Jia-Lin Zhu,[a] Li-Ming Tao[b] and Yong Ding*[a]*

[a] State Key Laboratory of Applied Organic Chemistry, College of Chemistry and Chemical Engineering, Lanzhou University, Lanzhou, Gansu 730000, China. [b] Key Laboratory of Science and Technology on Wear and Protection of Materials, Lanzhou Institute of Chemical Physics, Chinese Academy of Sciences, Lanzhou, Gansu 730000, China.

Email addresses: taolm@licp.cas.cn (Li-Ming Tao), dingyong1@lzu.edu.cn (Yong Ding)

Chemicals.

1,3,5-triformylbenzene, terephthaldehyde, 4,4'-biphenyldicarboxaldehyde, [1,1':4',1"-terphenyl]-4,4"-dicarboxaldehyde, 1,4-diaminobenzene, 1,3,5-Tris(4-aminophenyl)benzene, 1,3,5-Tris(4-aminophenoxy)benzene were purchased from Jilin Chinese Academy of Sciences - Yanshen Technology Co., Ltd. and used as received. Scandium(III) trifluoromethanesulfonate ($Sc(OTf)_3$) was purchased from TCI (Shanghai) Development Co., Ltd. and used as received. 1,4-dioxane, mesitylene, acetonitrile, methanol were purchased from J&K Scientific Ltd. (Beijing) and used without further purification.

Characterizations.

All of the as-synthesized COFs were conducted the basic characterization to confirm the successful synthesis.

X-ray diffraction (XRD) was recorded on a Smartlab SE X-ray diffractometer. Cu Kα as the radiation (λ=0.154 nm) and the radiation entrance slit width was 1 mm. All of the COF samples were observed using a continuous 2θ scan from 2.0 – 30 º (Omega =

1.0 º).

X-ray photoelectron spectroscopy (XPS) was recorded on a thermo scientific NEXSA X-ray photoelectron spectrometer.

Infrared spectra were recorded on a BRUKER V70 fourier transform infrared spectrometer. KBr tablet pressing method was employed to collect the IR spectra.

TEM images were got from a Tecnai G2 F20 U-TWIN microscope. TEM sample was prepared through drop-casting of the COF filtrate for twice.

SEM images were got from an Apreo S SEM microscope. The working distance was 18 mm and the accelerating voltage was 30 kV. SEM sample on a silicon substrate was prepared through drop-casting of the COF filtrate. The drop-casting procedure was kept that same as the sensor device preparation. 1 μL filtrate per drop and 10 drop-casting cycles were carried out.

Nitrogen adsorption experiments and micropore analysis were conducted at 77 K using Micromeritics ASAP 2020 HD88. COF samples were degassed at 90 °C for 12 hours before analysis. Surface areas were determined by BET adsorption models, and pore sizes distributions were determined by DFT models included in the instrument software.

Combustion elemental analysis was conducted on Vario EL III Elementar Analyser Systeme.

UV-Vis spectra was recorded on a UV-2550 UV spectrophotometer.

A CHI 660E electrochemical workstation was used to measure the resistance of the COF sensing layer between the Au interdigital electrodes on the ceramic substrate under air atmosphere and in NH_3 sensing process.

Synthesis of COF 1.

For the synthesis of COF 1, 0.15 mmol 1,4-diaminobenzene (DAB, 16.22 mg) and 0.10 mmol 1,3,5-triformylbenzene (TFB, 16.21 mg) were added in 4 mL 1,4-dioxane/mesitylene (4/1, v/v) mixture in a glass vial (10 mL). The mixture was then sonicated for several minutes until the monomers were fully dissolved. Then, 0.036 mmol (17.7 mg, 0.12 equivalent relative to amino groups) $Sc(OTf)_3$ was added into

reaction system and the reaction system was sonicated for 30 s immediately. After the introduction of $Sc(OTf)_3$ catalyst, a large number of yellow precipitate emerged immediately. After that, the reaction system was sealed with a plastic cap for 72 h at room temperature. The COF 1 precipitate was then gathered via centrifugation. To remove the unreacted monomers and catalyst, the as-obtained COF 1 precipitate was washed with CH_3OH several times (>10 times). And then, the COF 1 powder was collected after drying at 70 °C for 24 h in a vacuum oven. The as-obtained COF 1 powder was used and characterized directly without any post-treatment.

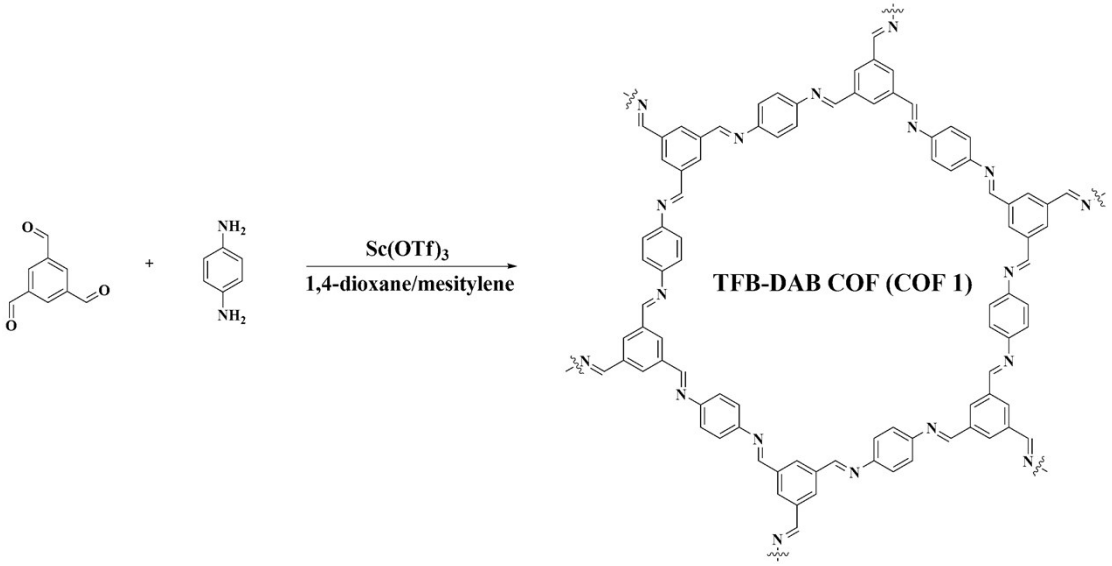

Scheme S1. Synthesis of COF 1.

Synthesis of COF 2.

For the synthesis of COF 2, 0.15 mmol terephthaldehyde (PDA, 20.12 mg) and 0.10 mmol 1,3,5-tris(4-aminophenyl)benzene (TAPB, 35.15 mg) were added in 4 mL 1,4-dioxane/mesitylene (4/1, v/v) mixture in a glass vial (10 mL). The mixture was then sonicated for several minutes until the monomers were fully dissolved. Then, 0.036 mmol (17.7 mg, 0.12 equivalent relative to amino groups) $Sc(OTf)_3$ was added into reaction system and the reaction system was sonicated for 30 s immediately. After the introduction of $Sc(OTf)_3$ catalyst, a large number of yellow precipitate emerged immediately. After that, the reaction system was sealed with a plastic cap for 72 h at

room temperature. The COF 2 precipitate was then gathered via centrifugation. To remove the unreacted monomers and catalyst, the as-obtained COF 2 precipitate was washed with CH_3OH several times (>10 times). And then, the COF 2 powder was collected after drying at 70 °C for 24 h in a vacuum oven. The as-obtained COF 2 powder was used and characterized directly without any post-treatment.

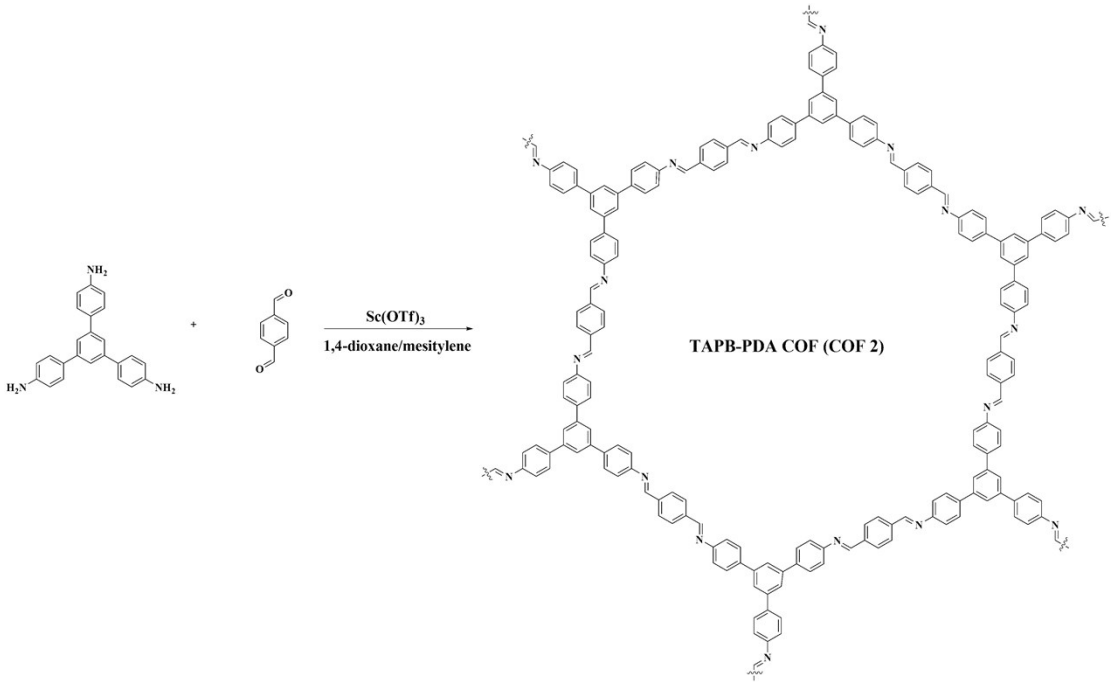

Scheme S2. Synthesis of COF 2.

Synthesis of COF 3.

For the synthesis of COF 3, 0.15 mmol 4,4'-biphenyldicarboxaldehyde (BPDA, 31.53 mg) and 0.10 mmol 1,3,5-tris(4-aminophenyl)benzene (TAPB, 35.15 mg) were added in 4 mL 1,4-dioxane/mesitylene (4/1, v/v) mixture in a glass vial (10 mL). The mixture was then sonicated for several minutes until the monomers were fully dissolved. Then, 0.036 mmol (17.7 mg, 0.12 equivalent relative to amino groups) $Sc(OTf)_3$ was added into reaction system and the reaction system was sonicated for 30 s immediately. After the introduction of $Sc(OTf)_3$ catalyst, a large number of yellow precipitate emerged immediately. After that, the reaction system was sealed with a

plastic cap for 72 h at room temperature. The COF 3 precipitate was then gathered via centrifugation. To remove the unreacted monomers and catalyst, the as-obtained COF 3 precipitate was washed with CH_3OH several times (>10 times). And then, the COF 3 powder was collected after drying at 70 °C for 24 h in a vacuum oven. The as-obtained COF 3 powder was used and characterized directly without any post-treatment.

For COF 3 sample catalyzed by 0.005, 0.02 and 0.06 equivalent $Sc(OTf)_3$ catalyst, the corresponding catalyst amount were 0.74 mg, 2.95 mg, 8.86 mg respectively. The other procedure were kept the same as that of COF 3 catalyzed by 0.12 equivalent $Sc(OTf)_3$ catalyst.

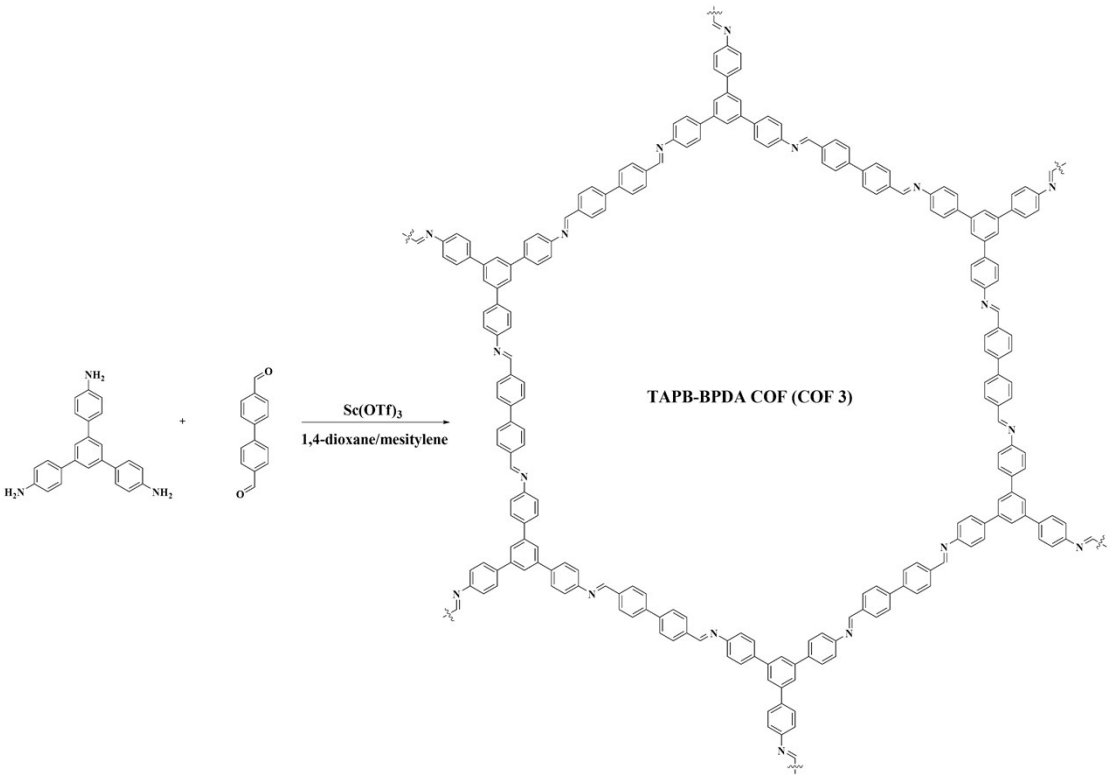

Scheme S3. Synthesis of COF 3.

Synthesis of COF 4.

For the synthesis of COF 4, 0.075 mmol [1,1':4',1"-terphenyl]-4,4"-dicarboxaldehyde (TPDA, 21.48 mg) and 0.05 mmol 1,3,5-tris(4-aminophenyl)benzene (TAPB, 17.57 mg) were added in 4 mL 1,4-dioxane/mesitylene (4/1, v/v) mixture in a glass vial (10

mL). The mixture was then sonicated for several minutes until the monomers were fully dissolved. Then, 0.036 mmol (17.7 mg, 0.24 equivalent relative to amino groups) $Sc(OTf)_3$ was added into reaction system and the reaction system was sonicated for 30 s immediately. After the introduction of $Sc(OTf)_3$ catalyst, a large number of yellow precipitate emerged immediately. After that, the reaction system was sealed with a plastic cap for 72 h at room temperature. The COF 4 precipitate was then gathered via centrifugation. To remove the unreacted monomers and catalyst, the as-obtained COF 4 precipitate was washed with CH_3OH several times (>10 times). And then, the COF 4 powder was collected after drying at 70 °C for 24 h in a vacuum oven. The as-obtained COF 4 powder was used and characterized directly without any post-treatment.

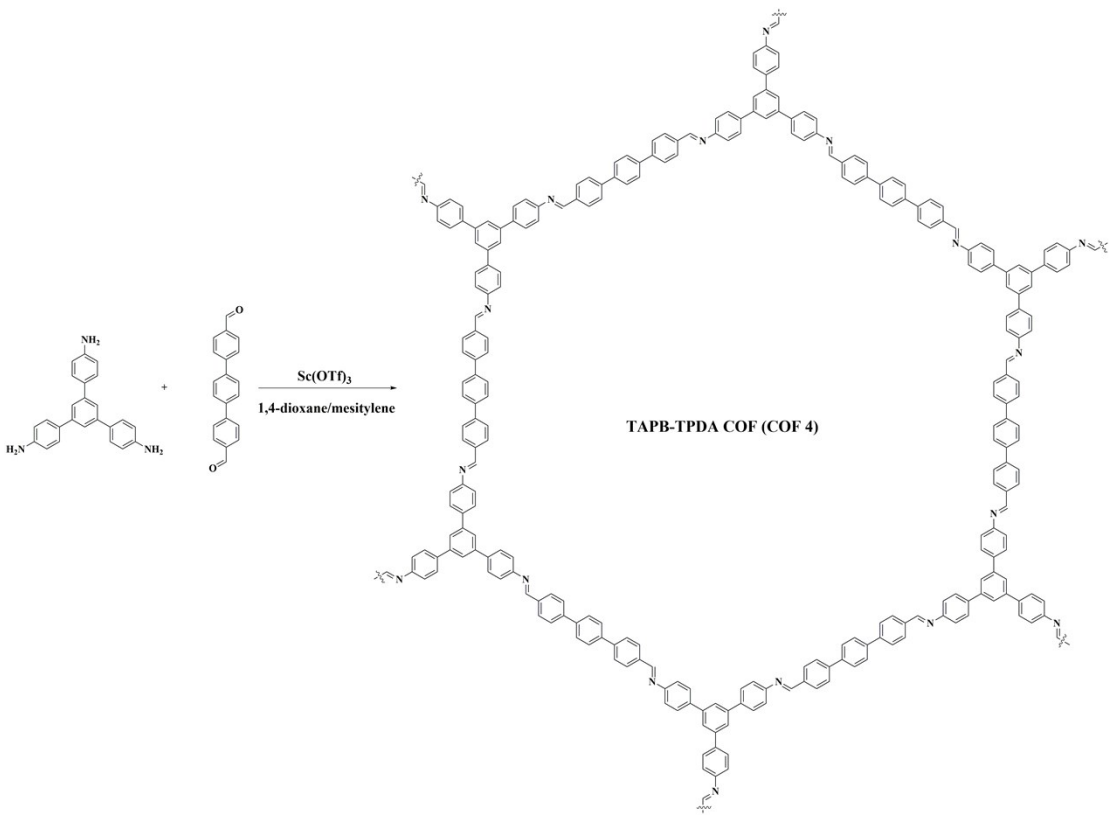

Scheme S4. Synthesis of COF 4.

Synthesis of COF 5.

For the synthesis of COF 5, 0.15 mmol terephthaldehyde (PDA, 20.12 mg) and 0.10 mmol 1,3,5-tris(4-aminophenoxy)benzene (TAPOB, 39.95 mg) were added in 4 mL

1,4-dioxane/mesitylene (4/1, v/v) mixture in a glass vial (10 mL). The mixture was then sonicated for several minutes until the monomers were fully dissolved. Then, 0.036 mmol (17.7 mg, 0.12 equivalent relative to amino groups) $Sc(OTf)_3$ was added into reaction system and the reaction system was sonicated for 30 s immediately. After the introduction of $Sc(OTf)_3$ catalyst, a large number of light yellow precipitate emerged immediately. After that, the reaction system was sealed with a plastic cap for 72 h at room temperature. The COF 5 precipitate was then gathered via centrifugation. To remove the unreacted monomers and catalyst, the as-obtained COF 5 precipitate was washed with CH_3OH several times (>10 times). And then, the COF 5 powder was collected after drying at 70 °C for 24 h in a vacuum oven. The as-obtained COF 5 powder was used and characterized directly without any post-treatment.

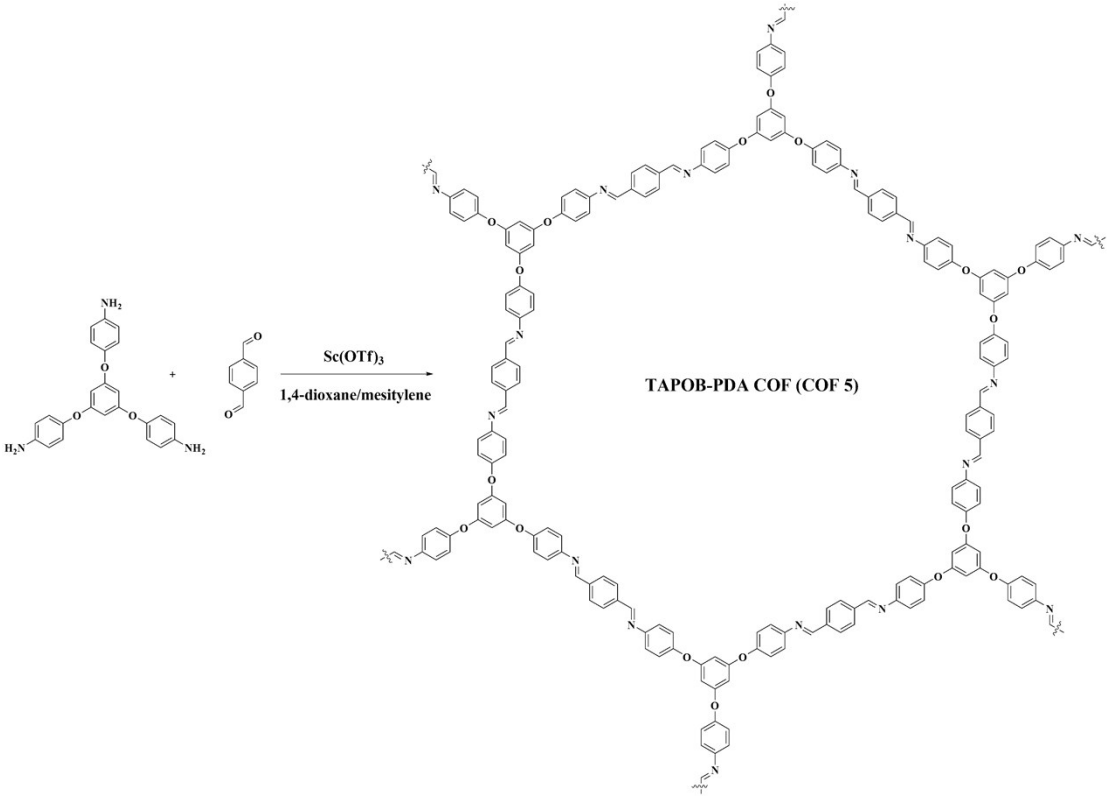

Scheme S5. Synthesis of COF 5.

DFT calculations.

In order to further study the sensing mechanism of imine-linked COF to NH_3, we

chose a structural fragment of imine-linked COF ring as the model molecule to explore the interaction between NH_3 molecule and imine-linked COF. Geometry optimization was carried out using DFT/B3LYP method in Gaussian 09W computational chemistry program based on 6-31G basis set.[1,2] In order to easy comparison with the experimental results, all of the as-obtained computational results were the data at 25 °C. Generally, individual molecules, including NH3 and the model molecule of imine-linked COF, were optimized. After that, these two molecules were put together and calculated again. Several fundamental features for optimized geometry, such as bond length, molecule orbitals (MOs), Mulliken charge distribution, and also the minimized energy values could be obtained.[3-5] To comparison, CO and the corresponding complex composed of CO and the imine-linked COF model molecule were also calculated. All of these computational results had been listed in Table S1. Figure S15 exhibited the top view and the side view of the optimized structures.

Table S2 listed the adsorption energy, shortest atom-to-atom distance and the Mulliken charge on gas molecules during the adsorption process of NH_3 on imine-linked COF model molecule as well as the CO on imine-linked COF model molecule.

The UV-Vis spectra of N-benzylideneaniline ($C_{13}H_{11}N$) and N-benzylideneaniline/NH3 complex were also calculated by DFT/B3LYP method in Gaussian 09W computational chemistry program based on 6-31G basis set. Figure S16a and b showed the optimized structures of N-benzylideneaniline and N-benzylideneaniline/NH_3 complex. The calculated UV-Vis spectra of N-benzylideneaniline and N-benzylideneaniline/NH_3 complex were plotted in Figure S16c. The absorption peak of N-benzylideneaniline at 326 nm red shifted to 370 nm after NH_3 adsorbed on.

Preparation of sensor device.

For the sensor device preparation, an interdigital Au electrode with a distance of about 100 μm on ceramic substrate (10×10 mm) was used. 2 mg imine-linked COF powder was added into 2 ml CH_3CN and the mixture was sonicated for 30 min continuously

to form a suspension. This suspension was then filtrated using a millipore filter (PVDF, Φ=0.45μm) to remove the particles with large size. The filtrate contained small size COF particles, which looked like colloid solution, was then collected and dropped on Au interdigital electrodes on ceramic substrate. After drying in air, the COF filtrate was dropped on the Au interdigital electrodes once again. The liquid volume of the COF filtrate that dropped on Au interdigital electrodes per time was kept a minimum value (1 μL) to ensure that only the Au interdigital electrodes were covered by the COF filtrate. This procedure needed to be repeated several cycles (5-20 cycles) until the sensor device showed a constant resistance value.

The preparation procedure for all of the sensor device were the same except for the COF sample. It should be noted that the drop-casting times for COFs with good conductivity were smaller than that of COFs with poor conductivity. For COF 3 (0.12 equiv. $Sc(OTf)_3$ catalyzing), COF 2 and COF 4, ten times drop-casting could led to a constant sensor resistance. However, for COF 1, COF 5 and COF 3 (0.005 equiv. $Sc(OTf)_3$ catalyzing), many times drop-casting were needed. Generally, bigger than 20 times.

In order to preparation of the sensor device with COF 3 (0.12 equiv. $Sc(OTf)_3$ catalyzing) powder sample, we mixed 5 mg COF 3 powder with 0.5 mL CH_3CN in a agate mortar and ground thoroughly. After 5 min of grinding, the COF 3 slurry was transferred on the Au interdigital electrodes using a tube. A thick COF 3 layer on the Au electrodes was formed after evaporation of CH_3CN (Figure S14).

In-situ UV-Vis experiment.

For in-situ UV-Vis experiment of N-benzylideneaniline, 1 mg N-benzylideneaniline was dissolved into 3 mL CH_3CN to form a solution. After that, the UV-Vis spectra was recorded on a UV-2550 UV spectrophotometer from 185 nm to 500 nm. Immediately, the NH_3 was introduced in the N-benzylideneaniline solution through NH_3 bubbling. The corresponding UV-Vis spectra of N-benzylideneaniline/NH_3 complex was collected during the NH_3 bubbling process. CH_3CN was used as the reference solution in above experiments.

For in-situ UV-Vis experiment of COF 3, 2 mg imine-linked COF 3 powder was added into 2 ml CH_3CN and the mixture was sonicated for 30 min continuously to form a suspension. This suspension was then filtrated using a millipore filter (PVDF, Φ=0.45μm) to remove the particles with large size. The filtrate contained small size COF 3 particles, which looked like a colloid solution, was then collected. The UV-Vis spectra of COF 3 filtrate was recorded on a UV-2550 UV spectrophotometer from 185 nm to 500 nm. Immediately, the NH_3 was introduced in the COF 3 filtrate through NH_3 bubbling. The corresponding UV-Vis spectra of COF 3/NH_3 complex was collected during the NH_3 bubbling process. CH_3CN was used as the reference solution in above experiments.

Band-structure test.

For band structure test, we collected the UV-Vis diffuser reflectance spectra and Mott-Schottky plots of COF 3, respectively.

UV-Vis diffuser reflectance spectra was recorded on a UV-2550 UV spectrophotometer. The diffuse reflectance attachment, integrating sphere (60 mm), was used for removing the light scattering effect. $BaSO_4$ was used as the reference.

Mott-Schottky plots were recorded on CHI 660E electrochemical workstation with a standard three-electrode system. The COF 3-coated ITO was the working electrode, Pt plate was the counter electrode and the Hg/Hg_2Cl_2 electrode was reference electrode. A 0.2 M Na_2SO_4 solution (pH = 6.8) was used as the electrolyte. The applied potentials vs. Hg/Hg_2Cl_2 is converted to RHE potentials using the following equation:

$$E_{RHE} = E_{Hg/Hg2Cl2} + 0.0591pH + E_{Hg/Hg2Cl2} \ (E_{Hg/Hg2Cl2} = 0.242\ V)$$

For COF 3-coated ITO preparation, indium-tin oxide (ITO) glasses were firstly cleaned by sonication in ethanol for 30 min and dried under nitrogen flow. Then, COF 3 filtrate was drop-casted on the ITO surface directly until a visible light yellow COF membrane emerged. For COF 3 prepared from 0.12 equivalent $Sc(OTf)_3$ catalyst, only the COF 3 filtrate was drop-casted on. For COF 3 prepared from 0.005, 0.02 and 0.06 equivalent $Sc(OTf)_3$ catalyst, 10 μL 0.05 wt.% Nafion solution was also dropped on

after the drop-casting of COF 3 filtrate to prevent the fall off of COF 3. Immediately, the COF 3 coated ITO electrode was total dried in air.

PXRD simulation.

The Accelrys[6] Materials Studio (version 4.4) program suite was used to simulate the powder diffraction of COF 3. The initial structure was built from a hexagonal unit cell with a *P6/m* space group. The cell parameter was $a = b = 44.96$ Å and $c = 3.48$ Å determined by MS Reflex Plus module. The structures were optimized using the Geometry Optimization routine including energy minimization with cell parameters optimization using MS DMol3 module. Modeling of the staggered structures were also performed with a *P*3 unit cell with a *c* parameter of 6.6 Å. The PXRD was calculated with the Reflex Plus module. The experimental data was applied to a Pawley refinement using the Pseudo-Voigt peak shape function.

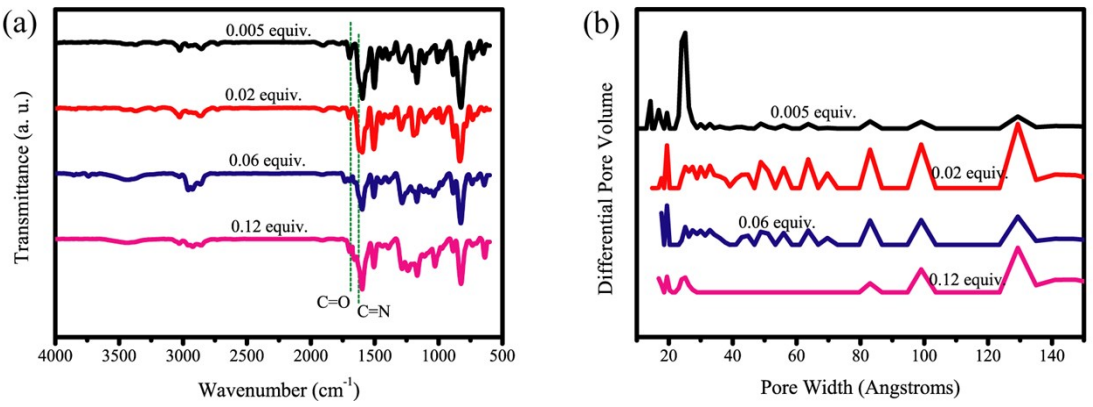

Fig. S1. (a) IR of COF 3 and (b) NLDFT calculated pore size distributions of COF 3 catalyzed by different equivalent of $Sc(OTf)_3$ catalyst.

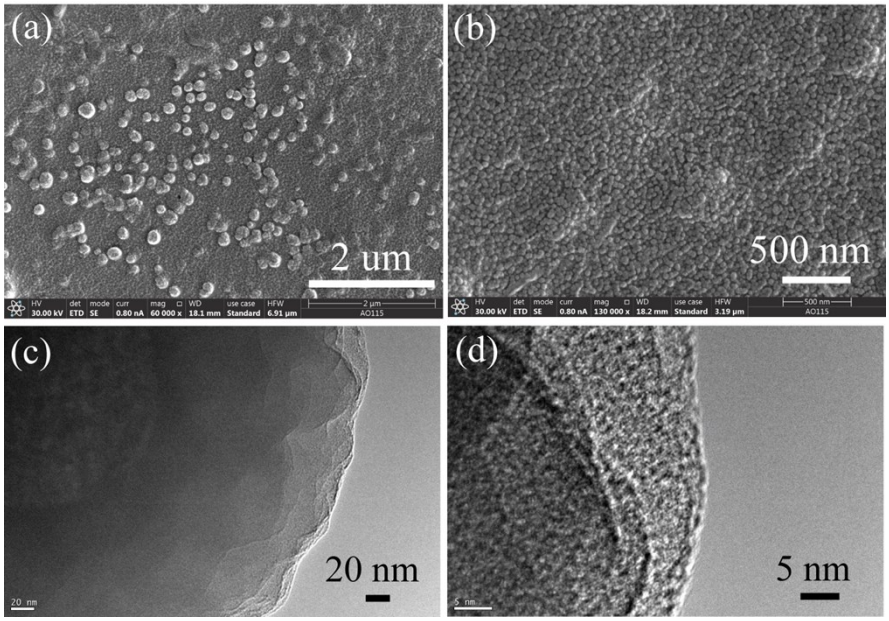

Fig. S2. (a), (b) SEM images, (c) TEM and (d) HRTEM image of COF 3 (0.12 equiv. $Sc(OTf)_3$ catalyzed).

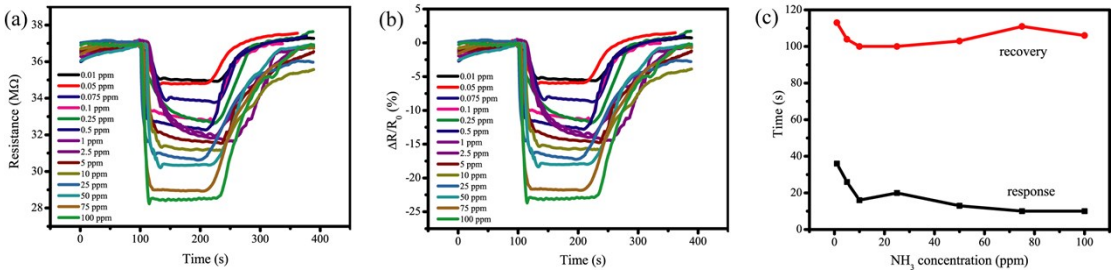

Fig. S3. Sensing results of COF 3 (0.12 equiv. $Sc(OTf)_3$ catalyzed) to NH_3 with various concentrations. (a) Plots of sensor resistance versus time. (b) Plots of response value versus time. (c) Response and recovery times of the sensor device prepared from COF 3 (0.12 equiv. $Sc(OTf)_3$ catalyzed) at different NH_3 concentrations.

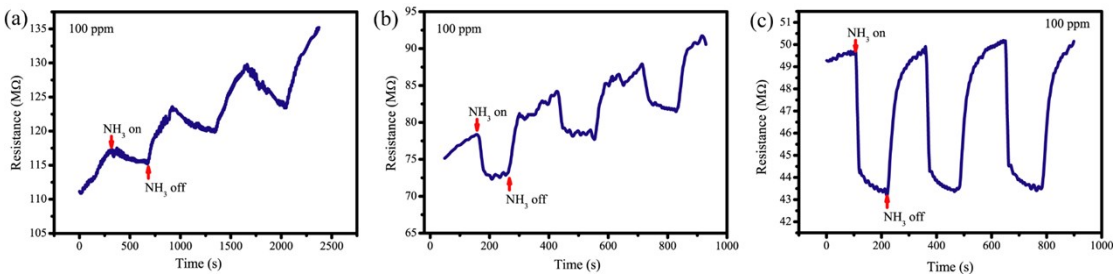

Fig. S4. NH_3 (100 ppm) sensing results of COF 3 prepared under (a) 0.005, (b) 0.02 and (c) 0.06 equivalent $Sc(OTf)_3$ catalyzing. Plots of sensor resistance versus time.

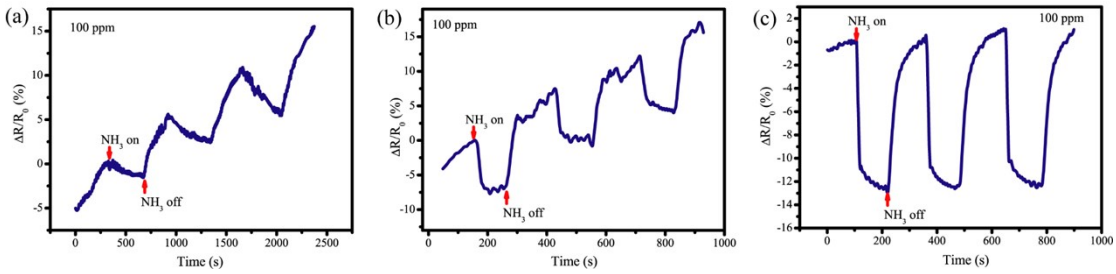

Fig. S5. NH_3 (100 ppm) sensing results of COF 3 prepared under (a) 0.005, (b) 0.02 and (c) 0.06 equivalent $Sc(OTf)_3$ catalyzing. Plots of response value versus time.

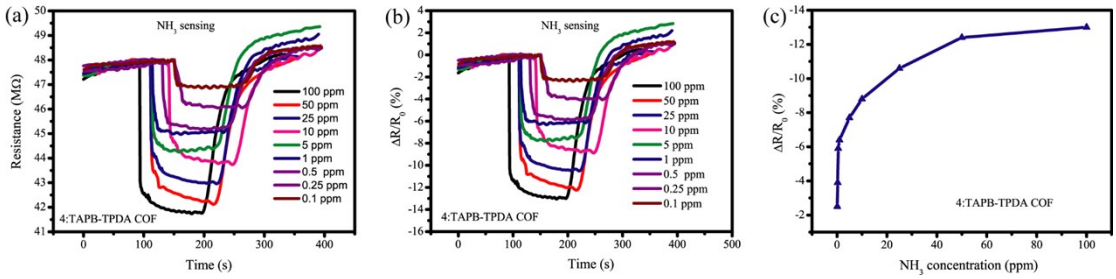

Fig. S6. Sensing results of COF 4 to NH_3 with various concentrations. (a) Plots of sensor resistance versus time. (b) Plots of response value versus time. (c) Plot of response value versus NH_3 concentration of COF 4.

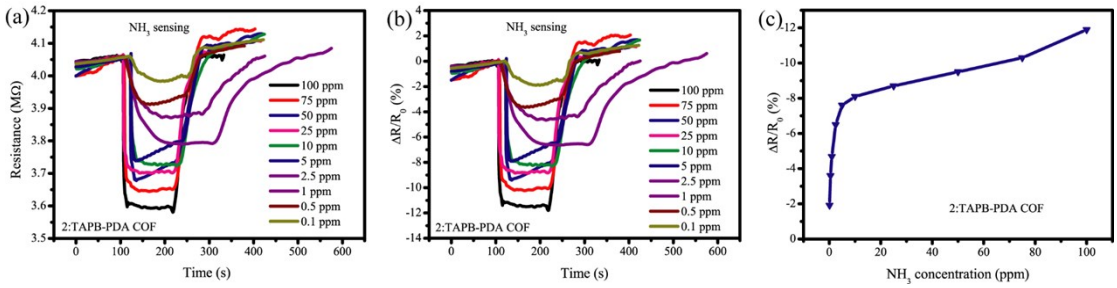

Fig. S7. Sensing results of COF 2 to NH_3 with various concentrations. (a) Plots of sensor resistance versus time. (b) Plots of response value versus time. (c) Plot of response value versus NH_3 concentration of COF 2.

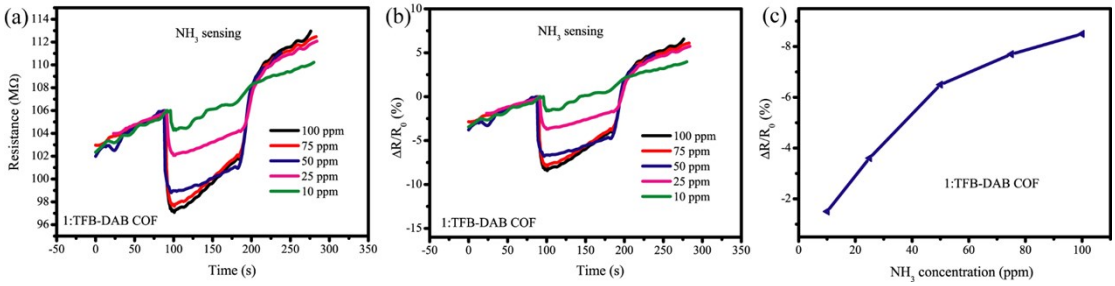

Fig. S8. Sensing results of COF 1 to NH_3 with various concentrations. (a) Plots of sensor resistance versus time. (b) Plots of response value versus time. (c) Plot of response value versus NH_3 concentration of COF 1.

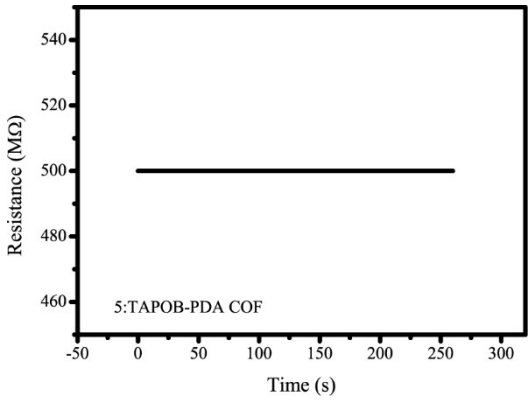

Fig. S9. Baseline resistance of sensor device that prepared from COF 5.

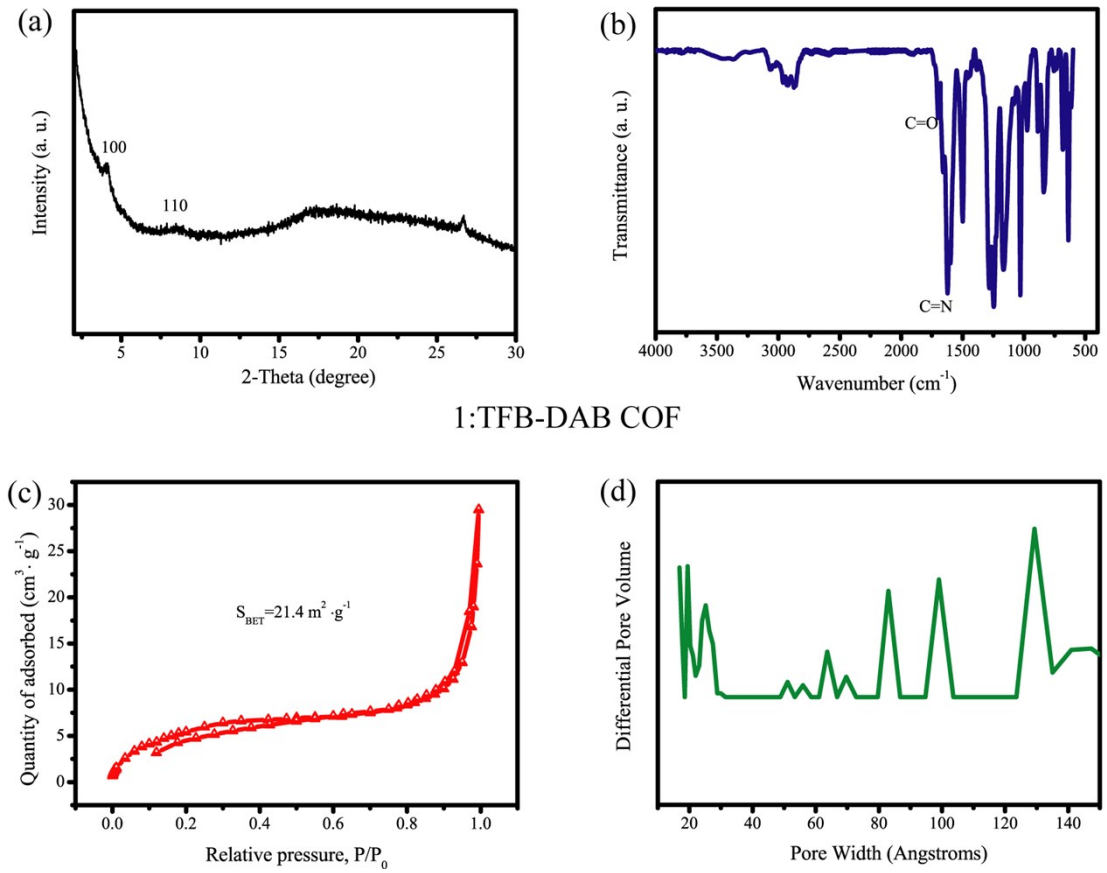

Fig. S10. (a) XRD, (b) IR, (c) N_2 adsorption-desorption isotherms and (d) NLDFT-calculated pore size distributions of COF 1.

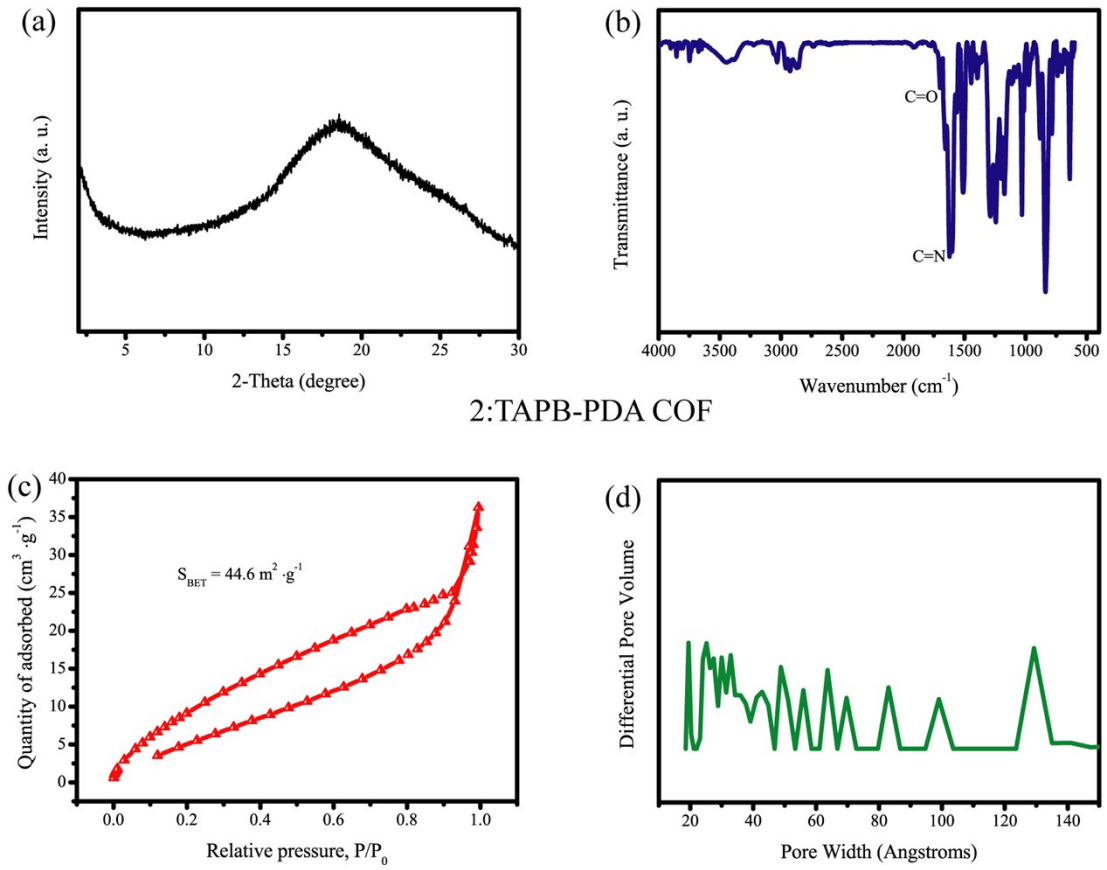

Fig. S11. (a) XRD, (b) IR, (c) N_2 adsorption-desorption isotherms and (d) NLDFT-calculated pore size distributions of COF 2.

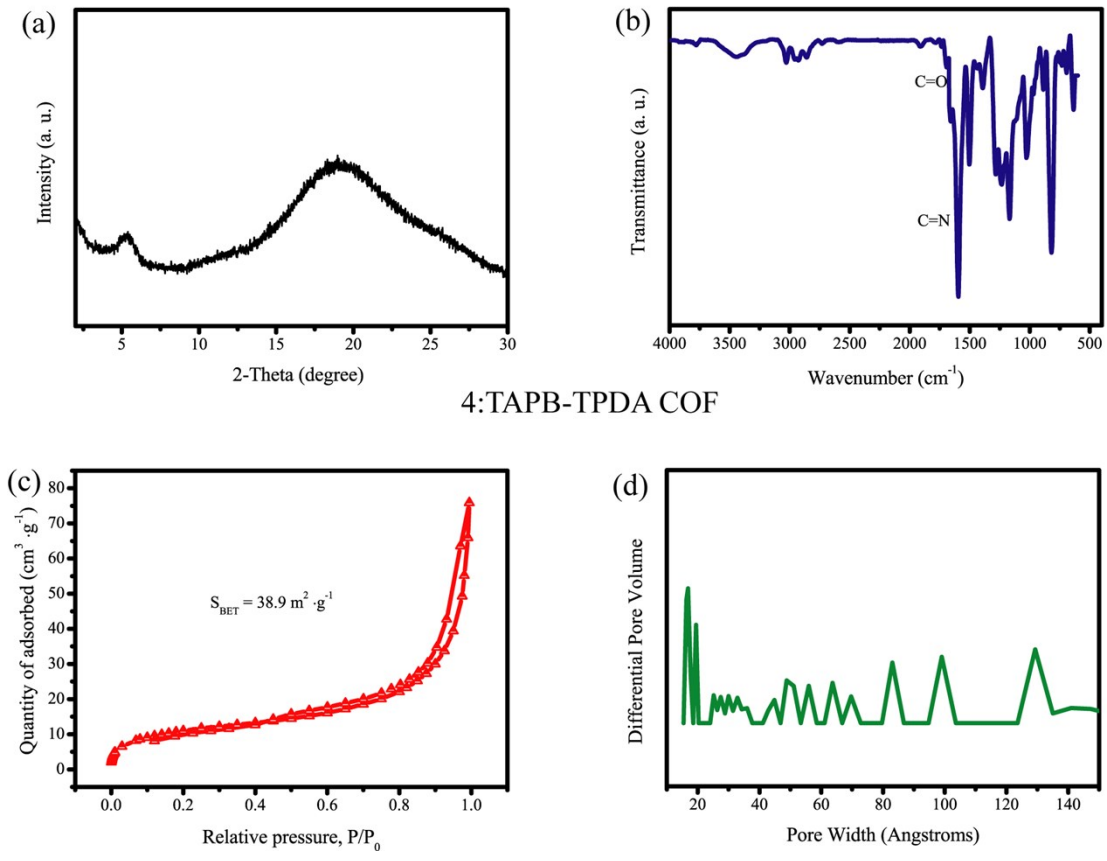

Fig. S12. (a) XRD, (b) IR, (c) N_2 adsorption-desorption isotherms and (d) NLDFT-calculated pore size distributions of COF 4.

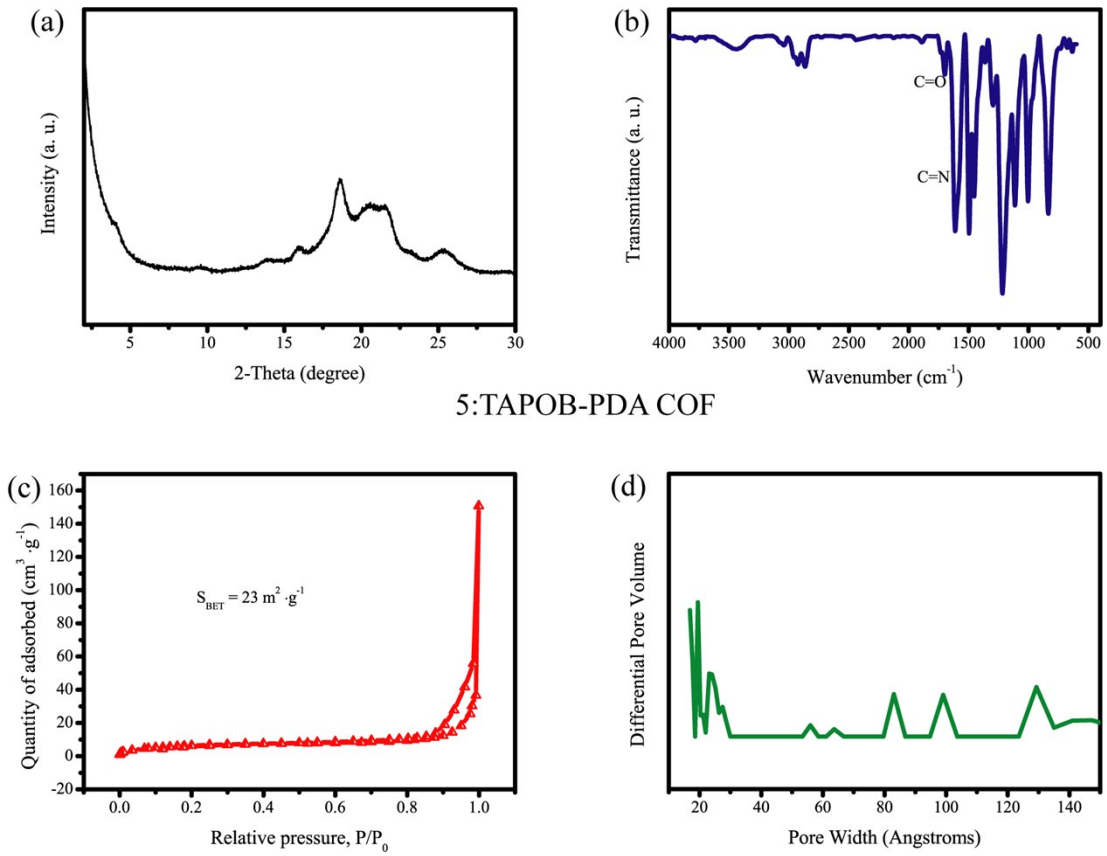

Fig. S13. (a) XRD, (b) IR, (c) N_2 adsorption-desorption isotherms and (d) NLDFT-calculated pore size distributions of COF 5.

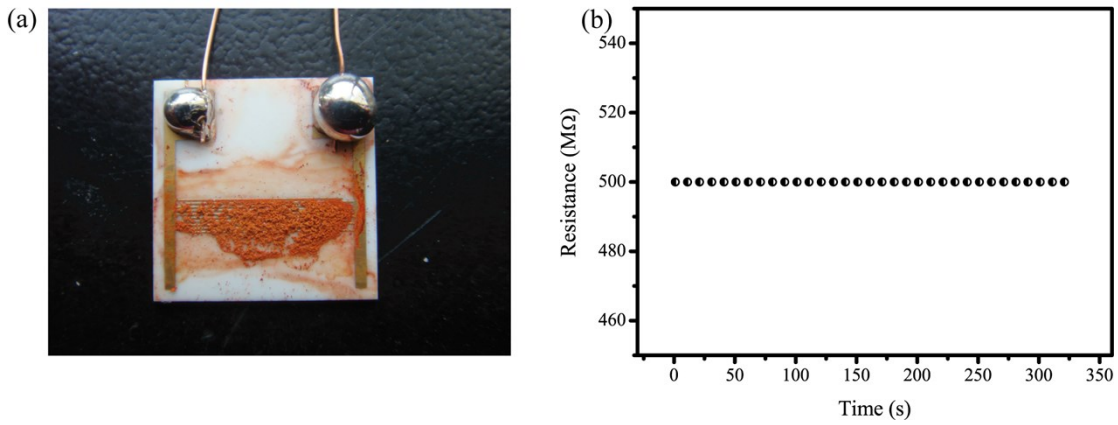

Fig. S14. (a) Photograph of the sensor device prepared from COF 3 powder sample

(catalyzed by 0.12 equiv. $Sc(OTf)_3$ catalyst) and (b) the baseline resistance of the as-prepared sensor device.

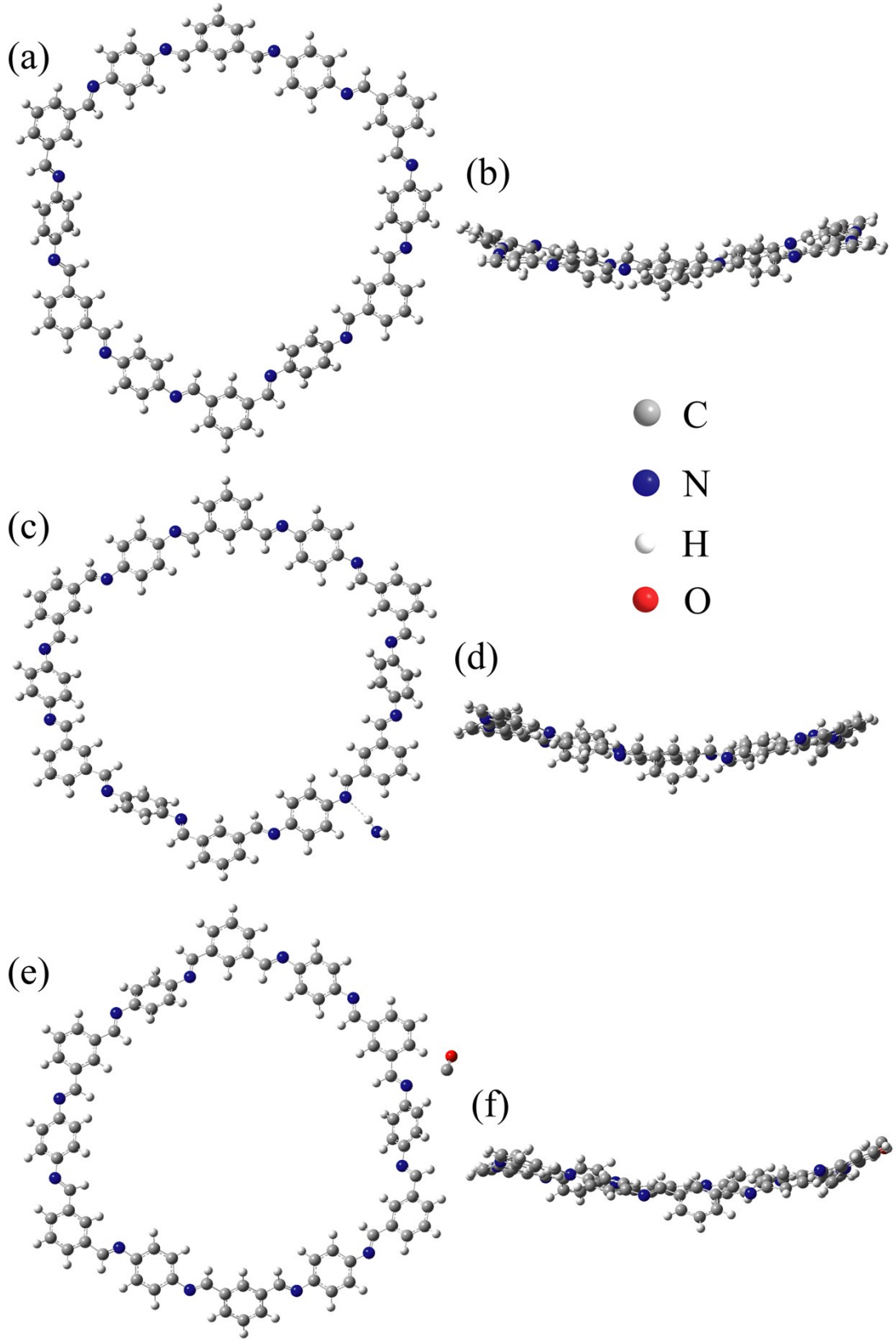

Fig. S15. Top view of the optimized structure of (a) imine-linked COF model

molecule and imine-linked COF model molecule with a (c) NH_3 and (e) CO molecule adsorbed on. Side view of the optimized structure of (b) imine-linked COF model molecule and imine-linked COF model molecule with a (d) NH_3 and (f) CO molecule adsorbed on.

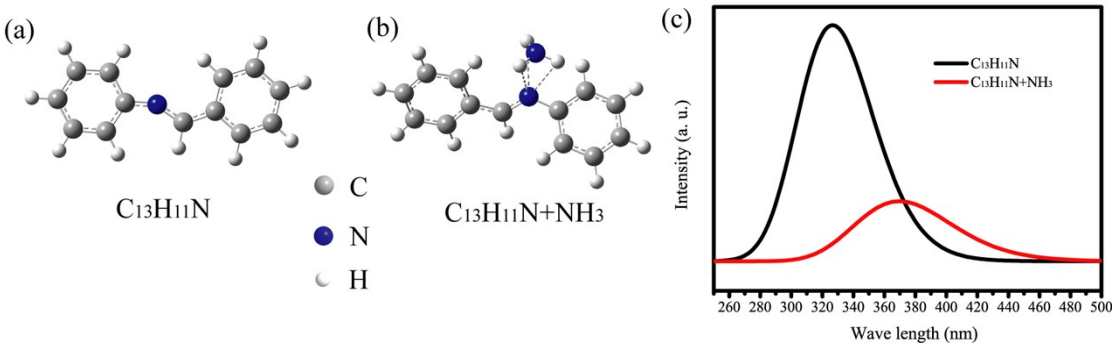

Fig. S16. The optimized structure of (a) N-benzylideneaniline and (b) N-benzylideneaniline with a NH_3 molecule adsorbed on. (c) Calculated red shift of the UV-Vis spectra during a hydrogen bonding process between N-benzylideneaniline and NH_3 molecule.

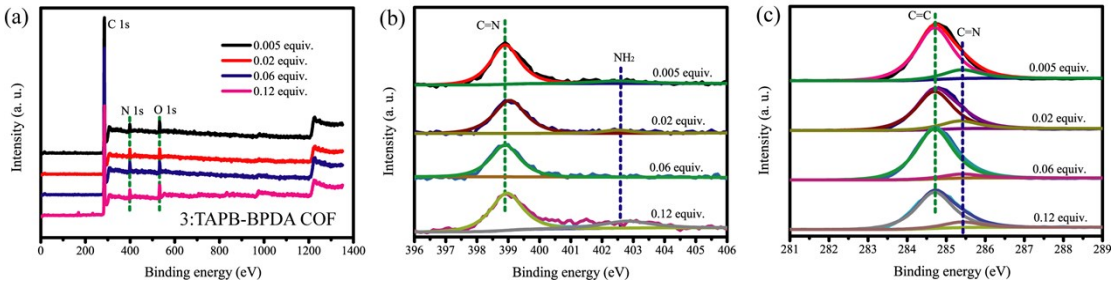

Fig. S17. (a) XPS survey, (b) N 1s and (c) C 1s XPS deconvolution results of COF 3 catalyzed by different equivalent of $Sc(OTf)_3$ catalyst.

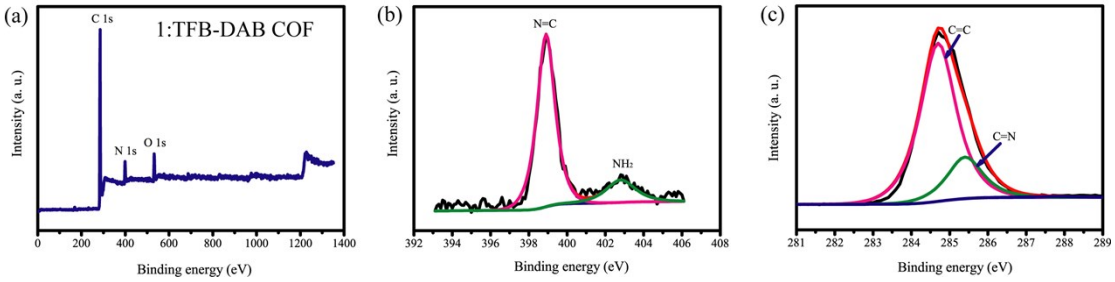

Fig. S18. (a) XPS survey, (b) N 1s and (c) C 1s XPS deconvolution results of COF 1.

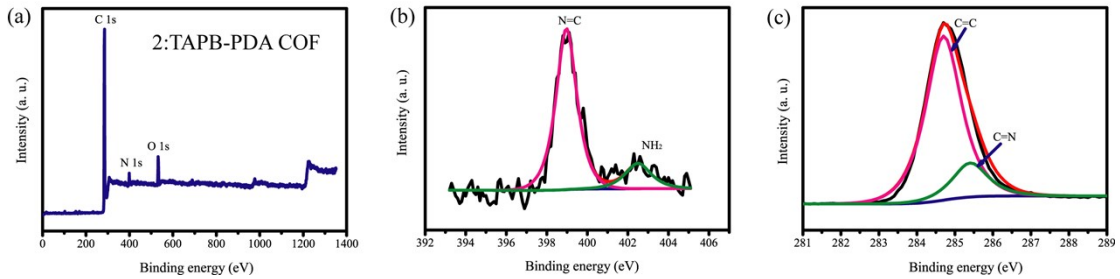

Fig. S19. (a) XPS survey, (b) N 1s and (c) C 1s XPS deconvolution results of COF 2.

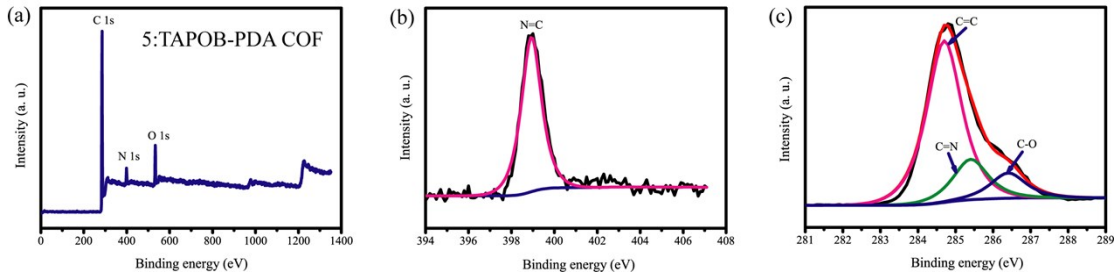

Fig. S20. (a) XPS survey, (b) N 1s and (c) C 1s XPS deconvolution results of COF 5.

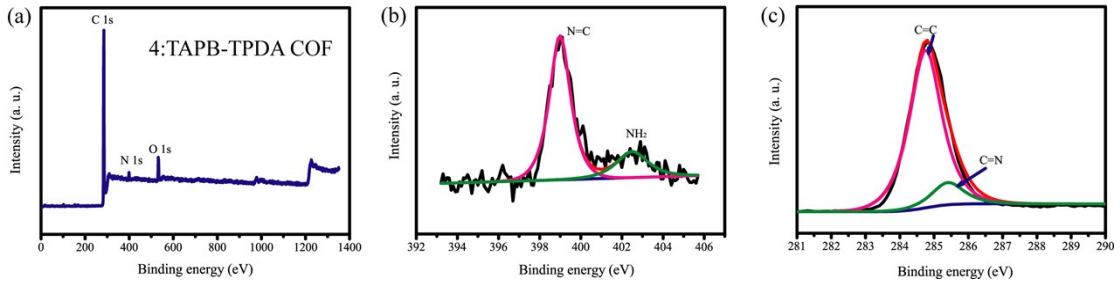

Fig. S21. (a) XPS survey, (b) N 1s and (c) C 1s XPS deconvolution results of COF 4.

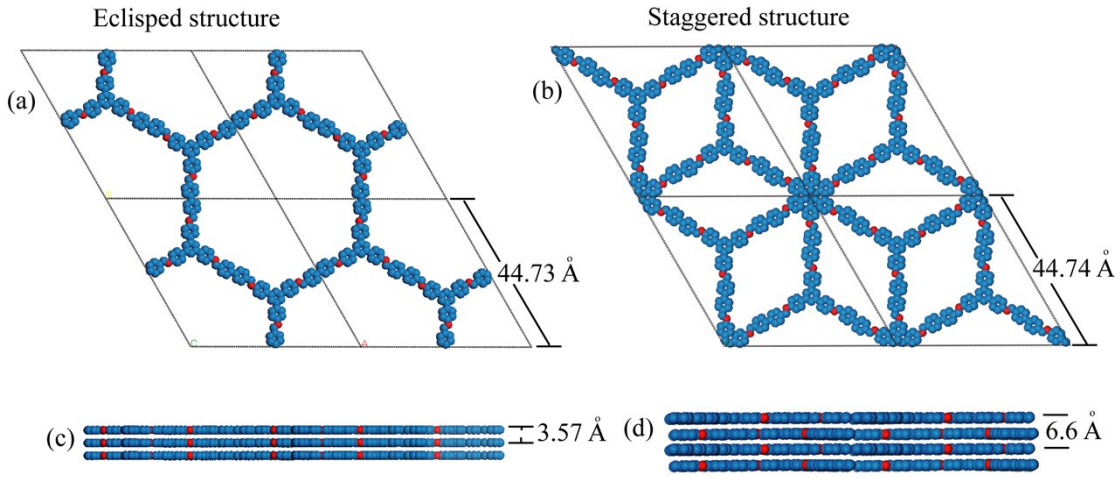

Fig. S22. (a) and (c) Eclipsed structure of COF 3 with the unit cell parameters

indicated. (b) and (d) Staggered structure of COF 3 with the unit cell parameters indicated. C: blue, N: red, and H atoms are omitted for clarity.

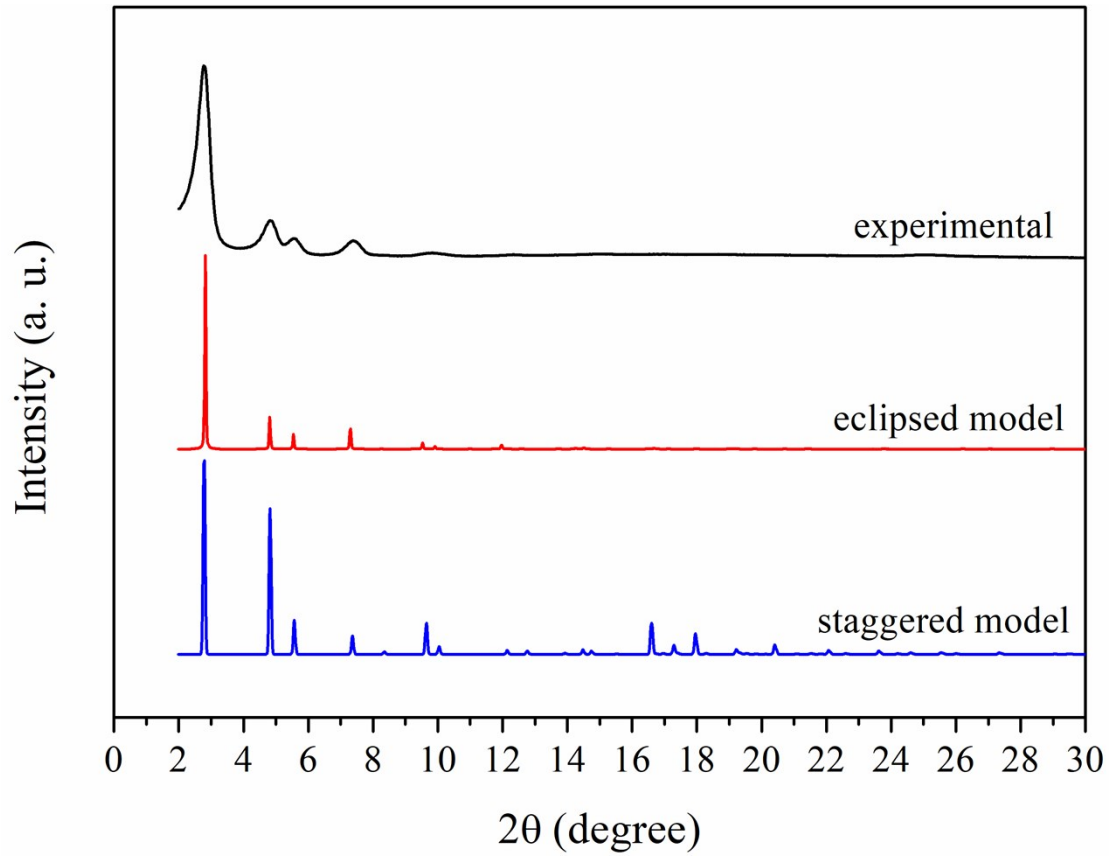

Fig. S23. Simulated PXRD spectra for COF 3 in eclipsed *P6/m* space group (red), in staggered (blue) *P*3 form and experimental data (black).

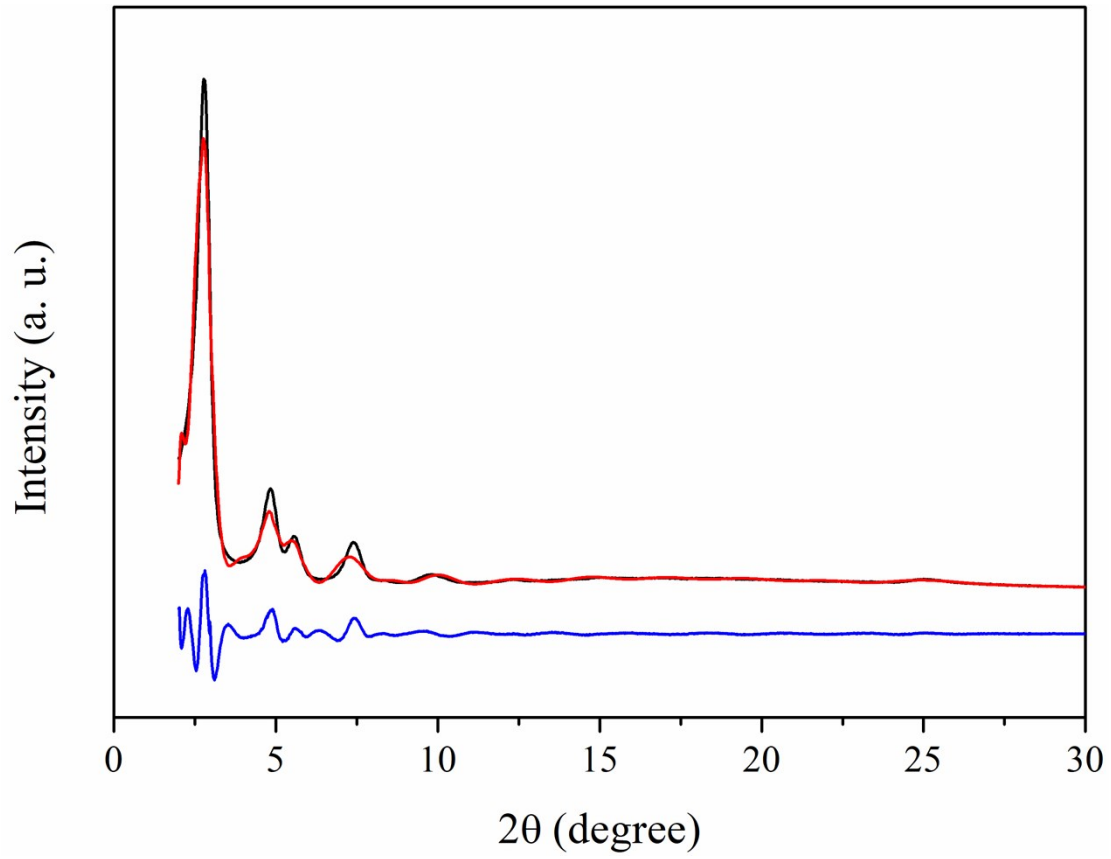

Fig. S24. Observed (black) and refined (red) PXRD profiles of COF 3 (0.005 equiv. $Sc(OTf)_3$ catalyzed) with an eclipsed arrangement, difference plot (blue, observed minus refined).

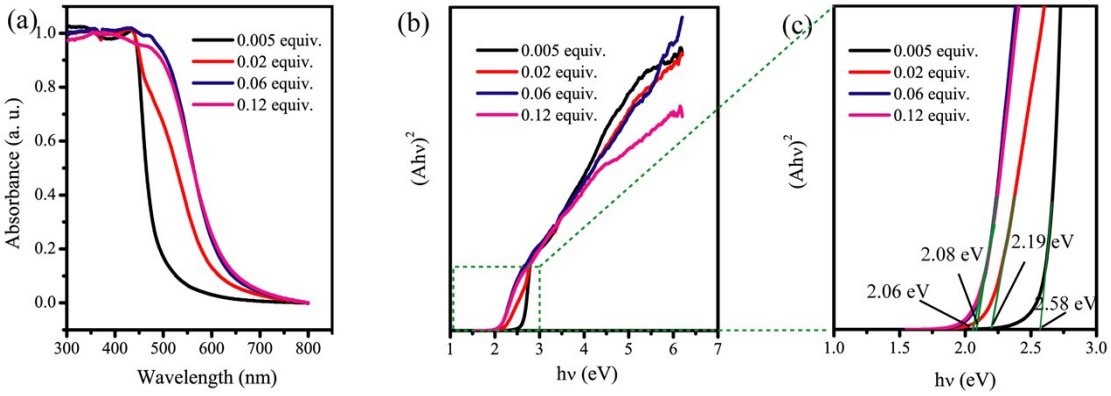

Fig. S25. (a) UV–vis reflectance spectra, (b) $(Ah\nu)^2$ versus hν curves and (c) the enlargement of the rectangular area in Fig. S25b of COF 3 catalyzed by 0.005 equiv., 0.02 equiv., 0.06 equiv. and 0.12 equiv. $Sc(OTf)_3$ catalyst.

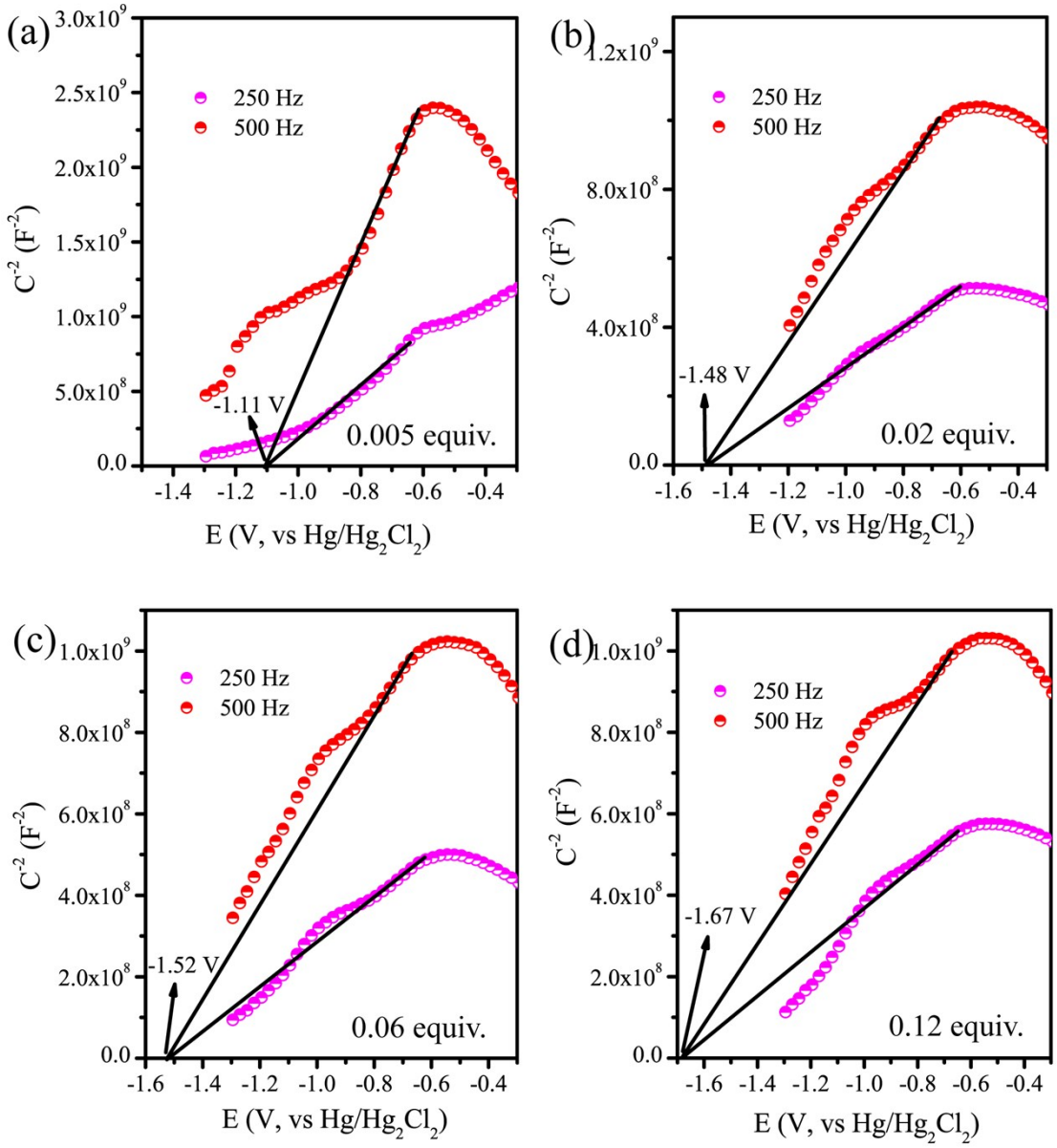

Fig. S26. Mott–Schottky plot of COF 3 catalyzed by (a) 0.005 equiv., (b) 0.02 equiv., (c) 0.06 equiv. and (d) 0.12 equiv. $Sc(OTf)_3$ catalyst.

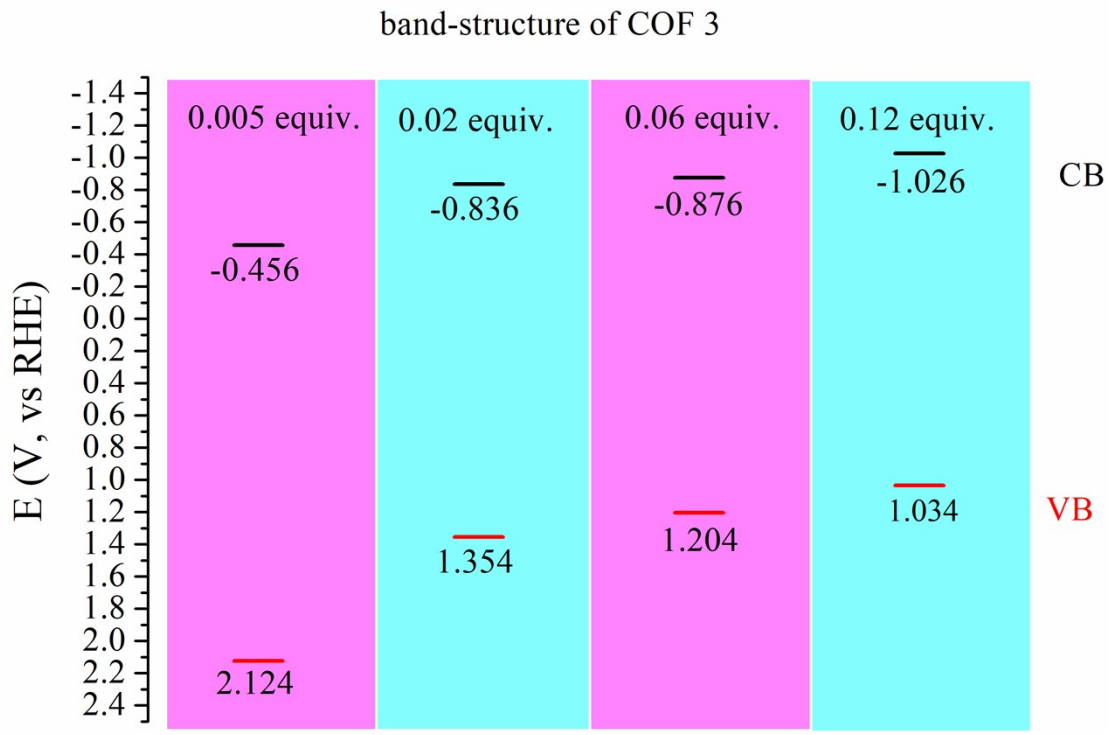

Fig. S27. Band-structure diagram for COF 3 catalyzed by 0.005 equiv., 0.02 equiv., 0.06 equiv. and 0.12 equiv. $Sc(OTf)_3$ catalyst.

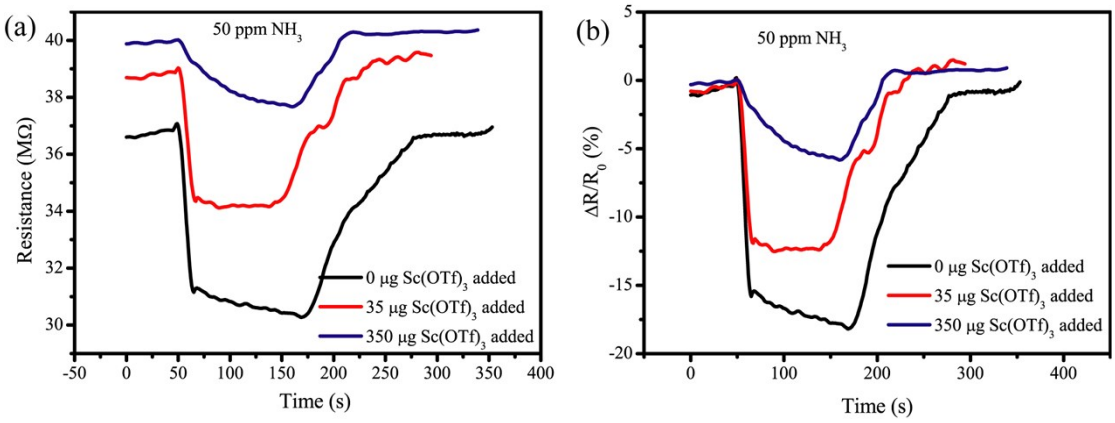

Fig. S28. Sensing results of COF 3 (catalyzed by 0.12 equivalent $Sc(OTf)_3$ catalyst) sensor with 0 μg, 35 μg and 350 μg additional $Sc(OTf)_3$ added. (a) Plots of resistance versus time. (b)Plots of response value versus time.

For further explore the affection of Sc residual to COF 3 (catalyzed by 0.12 equivalent $Sc(OTf)_3$) sensing ability, we measured its NH_3 sensing result with additional $Sc(OTf)_3$ drop-casted. We firstly prepared a $Sc(OTf)_3$ solution in ethanol

with a concentration of 3.5 mg/mL. Then 10 μL or 100 μL $Sc(OTf)_3$ solution were drop-casted (5 μL per drop) on the COF 3 sensing layer of an as-prepared sensor device. After totally drying, we obtained two sensor device of COF 3 (catalyzed by 0.12 equivalent $Sc(OTf)_3$) with 35 μg and 350 μg additional $Sc(OTf)_3$ added. We immediately measured the NH_3 (50 ppm) sensing performance of these two sensor devices and the results have been showed in Fig. S28. The sensor baseline resistance has slightly increased after additional $Sc(OTf)_3$ was drop-casted on. Compared to the response value (18 %) of COF 3 to 50 ppm NH_3 without any $Sc(OTf)_3$ added, the response values became sharply decreased after 35 μg and 350 μg additional $Sc(OTf)_3$ were added. This might because the $Sc(OTf)_3$ precipitate covered the sensing layer surface and prevented the NH_3 adsorption on COF 3. Obviously, the scandium residual does affect NH_3 sensing ability of COF 3, it will make its sensitivity to NH_3 decrease.

Table S1. The results of thermal enthalpies, free energies, HOMO and LUMO for individual molecules as well as the complex of imine-linked COF model molecule and NH_3, imine-linked COF model molecule and CO after geometry optimization by using DFT/B3LYP process. The band gap was calculated from E_{LUMO}-E_{HOMO}.

	thermal Enthalpies (kJ/mol)	Free Energies (kJ/mol)	E_{HOMO}(eV)	E_{LUMO}(eV)	Band gap (eV)
COF model molecule	-10215721	-10216270	-5.6526	-2.2562	3.3964
NH_3	-148296	-148354	-5.9786	2.3166	8.2952
COF model molecule/NH_3	-10364035	-10364605	-5.6534	-2.2669	3.3865
CO	-297284	-297343	-10.1395	-1.1287	9.0108
COF model molecule/CO	-10513589	-10513010	-5.6547	-2.2554	3.3993

Table S2. Adsorption energy (E_a), equilibrium distance (d) and Mulliken charge (Q) of NH_3 and CO adsorbed on imine-linked COF model molecule.

System	E_a (eV)[a]	Q(e)[b]	d(angstrom)[c]

COF model molecule/NH_3	-0.1871	0.012	2.1962
COF model molecule/CO	-0.0495	0.014	3.4136

[a.] E_a is defined as $E_a = E_{COF/NH3} - E_{COF} - E_{NH3}$, where E is the calculated thermal enthalpies. The same calculation procedure is applied for CO. [b.] d is defined as the shortest atom-to-atom distance between imine-linked COF model molecule and NH_3 or CO. [c.] Q is defined as the Mulliken charge on the gas molecules, and a positive number meant electrons transfer from gas molecules to the imine-linked COF model molecule.

Table S3. The atomic content of C, H, N and O in COF 1, COF 2, COF 3, COF 4, COF 5 obtained from theoretical calculation, elemental analysis and XPS survey.

	Calculated			Elemental analysis			XPS results		
COFs	C	N	H	C	N	H	C	N	O
COF 1	81.53	13.58	4.89	63.68	11.77	4.31	86.08	7.56	-
COF 2	87.12	7.82	5.06	76.54	7.41	4.84	88.44	4.6	-
COF 3	88.45	6.45	5.10	72.64	6.43	4.79	84.6	6.55	-
COF 4	89.38	5.49	5.13	75.29	4.87	4.78	92.69	3.51	-
COF 5	79.98	7.17	4.65	77.13	7.41	4.67	90.88	2.93	6.18

Table S4. The atomic content of C, H and N in COF 3 (catalyzed by different equivalent of $Sc(OTf)_3$ catalyst) obtained from theoretical calculation, elemental analysis and XPS survey.

	Calculated			Elemental analysis			XPS results	
COF 3	C	N	H	C	N	H	C	N
0.005 equiv.	88.45	6.45	5.10	85.79	6.51	5.31	92.69	3.51
0.02 equiv.	88.45	6.45	5.10	84.31	8.14	5.36	92.33	4.24
0.06 equiv.	88.45	6.45	5.10	83.35	5.87	5.21	92.78	3.79
0.12 equiv.	88.45	6.45	5.10	72.64	6.43	4.79	84.6	6.55

Table S5. The baseline resistance of the sensor device prepared from different COFs.

Sensor device	COF 1	COF 2	COF 4	COF 5	COF 3			
					0.005 e[a]	0.02 e	0.06 e	0.12 e
Baseline resistance(MΩ)	106	4.1	48	500	117	78	49.5	37

[a] e stands for equivalent.

Table S6. The comparison of representative reported NH_3 gas sensor.

Sensing materials	NH_3 concentration (ppm)	Response value ($(R_g-R_a)/R_a$)	Response time	Recovery time	Reference
Imine linked COF	100	23%	8 s	100 s	This work
PANI/rGO	20	3.65%	50s	23s	7
PPy/rGO	1	4.5%	118 s	122 s	8
Au/PPy	1	2.3	7 s	7 s	9
WO_3/PANI	100	121%	32 s	390 s	10
PANI/TiO_2	117	5.6	18 s	58 s	11
ZnO/PANI	100	2.3	21 s	61 s	12
C/rGO–Co_3O_4	50	123%	20 s	360 s	13
Cu_2O /rGO	200	104%	28 s	206 s	14
PANI/FMWCNT	100	30	-	-	15
ZnO-T− CNT	100	350 (I_g/I_a)	56 s	61 s	16

Table S7. Fractional atomic coordinates for unit cell of COF 3 calculated using the Materials Studio modeling program after performing the Pawley refinement.

Space group symmetry *P6/m*, R_p=7.5%, R_{wp}=9.3%
a=b=44.7306 Å, c=3.5746 Å, alpha=beta=90°, gamma=120°.

Atom	x	y	z
C1	0.34911	0.70220	0.00000
C2	0.36882	0.68582	0.00000
C3	0.37423	0.63282	0.00000
C4	0.41038	0.65256	0.00000
C5	0.43033	0.63658	0.00000
C6	0.41454	0.60064	0.00000
C7	0.37841	0.58073	0.00000
C8	0.35847	0.59672	0.00000
N9	0.43572	0.58505	0.00000
C10	0.42327	0.55197	0.00000
C11	0.44589	0.53709	0.00000
C12	0.43120	0.50127	0.00000
C13	0.45224	0.48646	0.00000
C14	0.48830	0.50730	0.00000
C15	0.50285	0.54328	0.00000
C16	0.48183	0.55809	0.00000

References

1 Ullah, H.; Rauf, A.; Ullah, Z.; Fazl-i-Sattar, Anwar, M.; Shah, A. A.; Uddin, G.; Ayub, K., Density functional theory and phytochemical study of Pistagremic acid, Spectrochimica Acta Part A Mol. Biomol. Spectrosc., 2014, 118, 210–214.

2 Hossain, M. A.; Jewaratnam, J.; Ramalingam, A.; Sahu, J. N.; Ganesan, P., A DFT method analysis for formation of hydrogen rich gas from acetic acid by steam reforming process, Fuel, 2018, 212, 49–60.

3 Rastegar, S. F.; Peyghana, A. A.; Ghenaatian, H. R.; Hadipour, N. L., NO_2 detection by nanosized AlN sheet in the presence of NH_3: DFT studies, Appl. Surf. Sci., 2013, 274, 217–220.

4 Beheshtian, J.; Peyghan, A. A.; Noei, M., Sensing behavior of Al and Si doped BC_3 graphenes to formaldehyde, Sens. Actuat. B, 2013, 181, 829–834.

5 Aghaei, S. M.; Monshi, M. M.; Torres, I.; Zeidi, S. M. J.; Calizo, I., DFT study of adsorption behavior of NO, CO, NO_2, and NH_3 molecules on graphene-like BC_3: A search for highly sensitive molecular sensor, Appl. Surf. Sci., 2018, 427, 326–333.

6 Materials Studio Release Notes v.4.4, Accelrys Software, San Diego, 2008.

7 Wu, Z. Q.; Chen, X. D.; Zhu, S. B.; Zhou, Z. W.; Yao, Y.; Quan, W.; Liu, B., Enhanced sensitivity of ammonia sensor using graphene/polyaniline nanocomposite, Sens. Actuat. B Chem., 2013, 178, 485–493.

8 Shen, W. S.; Shih, P.-J.; Tsai, Y.-C.; Hsu. C.-C.; Dai, C.-L., Low-concentration ammonia gas sensors manufactured using the CMOS–MEMS technique, Micromachines, 2020, 11, 92.

9 Li, Z. Y.; Chen, J. Y.; Chen, L.; Guo, M. L.; Wu, Y. P.; Wei, Y.; Wang, J. F.; Wang, X. G., Hollow Au/polypyrrole capsules to form porous and neural network-like nanofibrous film for wearable, super-rapid, and ultrasensitive NH_3 sensor at room temperature, ACS Appl. Mater. Interfaces, 2020, 12, 55056−55063.

10 Kulkarnia, S. B.; Navalea, Y. H.; Navaleb, S. T.; Stadlerb, F. J.; Ramgirc, N. S.; Patila, V. B., Hybrid polyaniline-WO_3 flexible sensor: A room temperature competence towards NH_3 gas, Sens. Actuat. B Chem., 2019, 288, 279–288.

11 Tai, H. L.; Jiang, Y. D.; Xie, G. Z.; Yu, J. S.; Chen, X., Fabrication and gas sensitivity of polyaniline–titanium dioxide nanocomposite thin film, Sens. Actuat. B Chem., 2007, 125, 644-650.

12 Das, M.; Sarkar, D., One-pot synthesis of zinc oxide - polyaniline nanocomposite for fabrication of efficient room temperature ammonia gas sensor, *Ceramics International,* 2017**,** 43, 11123-11131.

13 Feng, Q. X.; Zeng, Y. M.; Xu, P. C.; Lin, S. W.; Feng, C.; Li, X. G.; Wang, J., Tuning the electrical conductivity of amorphous carbon/reduced graphene oxide wrapped-Co_3O_4 ternary nanofibers for highly sensitive chemical sensors, J. Mater. Chem. A, 2019, 7, 27522-27534.

14 Meng, H.; Yang, W.; Ding, K.; Feng, L.; Guan, Y. F., Cu_2O nanorods modified by reduced graphene oxide for NH_3 sensing at room temperature, J. Mater. Chem. A, 2015, 3, 1174-1181.

15 Wan, P. B.; Wen, X. M.; Sun, C. Z.; Chandran, B. K.; Zhang, H.; Sun, X. M.; Chen, X. D., Flexible transparent films based on nanocomposite networks of polyaniline and carbon nanotubes for high-performance gas sensing, Small, 2015, 11, 5409-5415.

16 Schütt, F.; Postica, V.; Adelung, R.; Lupan, O., Single and networked ZnO−CNT hybrid tetrapods for selective room-temperature high-performance ammonia sensors, ACS Appl. Mater. Interfaces, 2017, 9, 23107−23118.